ACS APPLIED MATERIALS & INTERFACES

Research Article

www.acsami.org

H_2O–EG-Assisted Synthesis of Uniform Urchinlike Rutile TiO_2 with Superior Lithium Storage Properties

Jun Song Chen, Yen Nan Liang, Yongmei Li, Qingyu Yan, and Xiao Hu*

School of Materials Science and Engineering, Nanyang Technological University, 50 Nanyang Avenue, Singapore 639798

Supporting Information

ABSTRACT: A facile green method to synthesize uniform nanostructured urchinlike rutile TiO_2 is demonstrated. Titanium trichloride was selected as the TiO_2 precursor, and a mixed solvent containing H_2O and ethylene glycol was used. By using this binary medium, the nucleation and crystal growth of rutile TiO_2 can be regulated, giving rise to very uniform urchinlike structures with tailorable sizes. As confirmed by the SEM and TEM analysis, large particles with dense aggregation of needle-like building blocks or small ones with loosely packed subunits could be obtained at different reaction conditions. The as-prepared samples were applied as the anode material for lithium-ion batteries, and they were shown to have superior properties with a high reversible capacity of 140 mA h g^{-1} at a high current rate of 10 C for up to 300 cycles, which is almost unmatched by other rutile TiO_2-based electrodes. A stable capacity of 88 mA h g^{-1} can also be delivered at an extremely high rate of 50 C, suggesting the great potential of the as-prepared product for high-rate lithium-ion batteries.

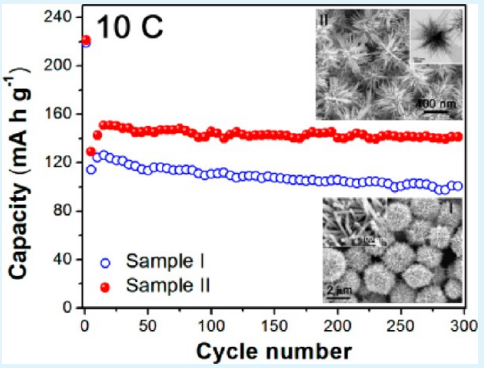

KEYWORDS: *urchinlike, rutile TiO_2, hydrothermal synthesis, green method, lithium-ion battery, high-rate performance*

INTRODUCTION

Great potentials of unique nanostructured materials have been demonstrated for many applications, including energy storage,[1−6] biology,[7] photocatalysis,[8,9] and so on. Titanium dioxide (TiO_2) is one of the intensively studied metal oxides, which has been widely used as the anode material for lithium-ion batteries.[10−14] Among the different polymorphs of the TiO_2 family, anatase is considered to be highly electrochemically active, while rutile is the most thermodynamically stable form.[15] Many studies have pointed out that the battery performance of bulk rutile TiO_2 is kinetically restricted by the anisotropic diffusion of Li^+ in the crystal structure; as the diffusion coefficient along the *c*-axis is much higher than that on the *ab*-plane.[16−19] Such issue can be alleviated by producing properly nanostructured rutile TiO_2.[20−22]

"Urchinlike" nanostructures are a distinct category of nanomaterials, and they are commonly shown as hierarchical spheres composed of one-dimensional (1D) building blocks pointing radially outward.[23−29] Compared to the analogous "dandelion-like" particles,[30,31] the subunits that construct urchinlike structures are thinner with a more loosely packed organization. To produce this type of nanostructure, many previous works utilized synthesis systems which contain titanium trichloride ($TiCl_3$) in a highly concentrated sodium chloride (NaCl) solution;[24,30,32−34] where Cl^- is believed to have certain structural directing effect. Potassium titanium oxide oxalate and hydrogen peroxide were also employed in some reported syntheses;[29,35] while in other works, dual precursors, that is, titanium tetrachloride ($TiCl_4$) and titanium(IV) *tert*-butoxide were incorporated in a single reaction system.[25,26] The urchinlike nanomaterials have also found applications in many important areas, including solar cell,[25,36,37] photocatalysis,[26,27] water treatment,[28] and lithium-ion batteries.[23,24,38,39] When it serves as the host for lithium storage, rutile TiO_2 experiences phase transition upon lithium insertion. A hexagonal structure of $R\bar{3}m$ will possibly be formed when it is at the fully intercalated state,[17] when a maximal lithium insertion coefficient of ~0.5 is reached.[22] This leads to a theoretical lithium storage capacity of about 170 mA h g^{-1}, which is comparable to that of anatase TiO_2.

However, the battery performance of rutile TiO_2 was still unsatisfactory[24] which is not only because of its intrinsic limitation mentioned above but also due to some extrinsic factors of the fabricated samples, including the lack of uniform size distribution and monodispersity. Thus, in order to improve the physicochemical properties of these advanced urchinlike TiO_2 nanomaterials, it is essential to design a more facile and environment-friendly synthesis method to overcome these drawbacks.

In this work, we proposed a green solvothermal method to synthesize uniform monodispersed urchinlike rutile TiO_2 without any surfactant. In the current system, $TiCl_3$ is selected as the TiO_2 precursor, and we use water and ethylene glycol (EG) as the solvent. The nucleation and crystal growth of rutile

Received: June 10, 2013
Accepted: September 10, 2013
Published: September 10, 2013

TiO_2 can be regulated in this binary medium, rendering samples with uniform size distribution. The volume ratio of H_2O and EG was found to have great influence on the product morphology, and the size of the urchinlike particles can also be tailored. Importantly, when the as-prepared sample was used as the anode material for lithium-ion batteries, the device demonstrated superior lithium storage properties as compared to those with other rutile TiO_2-based anodes tested under similar conditions. Specifically, a high reversible capacity of 140 mA h g^{-1} can be delivered at a high current rate of 10 C. The device can function for up to 300 charge−discharge cycles with excellent cyclic retention, which evidently shows the advantage of the samples obtained by our method.

EXPERIMENTAL SECTION

Material Preparation. Briefly, sample I was synthesized by adding 2 mL of $TiCl_3$ (~10 wt %, Sigma Aldrich) into a mixed solvent containing 3 mL of H_2O and 23 mL of EG. The solution was transferred into a Teflon-line stainless steel autoclave and put into an electric oven at 180 °C for 10 h. During this process, the Ti^{3+} ions will be oxidized into Ti^{4+} by the oxygen in the Teflon container and in the solvent. The autoclave was then left to cool down to room temperature. The yellowish white product was harvested by centrifugation and washed thoroughly with ethanol and water for several time, before drying at 60 °C overnight. Sample II was synthesized following the same procedure, except that 1 mL of $TiCl_3$ was added in the mixed solvent containing 8 mL of H_2O and 23 mL of EG.

Characterization. The morphology of the samples was studied by the field-emission scanning electron microscope (FESEM; JEOL, JSM-6700F, 5 kV) and transmission electron microscopy (TEM, JEOL, JEM-2100F, 200 kV). Crystallographic information of the samples was investigated with X-ray powder diffraction (XRD; Bruker, D8, Advance X-ray Diffractometer, Cu Kα, λ = 1.5406 Å). The N_2 adsorption and desorption isotherm was obtained at 77 K using Quantachrome Instruments, Autosorb AS-6B. Weight percentage of the organic compound in synthesized products was evaluated by the thermogravimteric analysis (TGA) under the air flow with a temperature ramp of 10 °C/min.

Electrochemical Measurements. The electrochemical measurements were performed on the CR2032 (3 V) coin-type cells with lithium metal as the counter/reference electrode. The electrolyte was prepared by dissolving1 M $LiPF_6$ into a mixture of ethylene carbonate (EC) and dimethyl carbonate (DMC) with weight ratio of 1:1. The working electrode was fabricated by mixing the active material (i.e., urchinlike TiO_2), conducting agent (carbon black, Super-P-Li) and binding agent (polyvinylidene fluoride) binder with the weight ratio of 70:20:10. Coin cells were assembled in an Ar-filled glovebox. Li-ion charge/discharge tests were performed on a NEWARE battery tester with the voltage window of 1−3 V.

RESULTS AND DISCUSSION

Figure 1 shows the morphology of the sample obtained at a low H_2O-to-EG volume ratio (sample I; see Experimental Section). It is evident from Figure 1A that the sample contains well-dispersed spherical particles with a diameter of about 2 μm. Under closer observation (Figure 1B), the particles are shown to have an urchinlike structure; with the nanoneedle subunits pointing radially outward. The inset of Figure 1B reveals that the nanoneedles are with a thickness of only a few nanometers. The transmission electron microscopy (TEM) image as included in Figure 1C shows that these 1D subunits are clearly identified at the circumferential regions of the particles, with a densely packed central domain. The ultrathin feature and smooth surface of the nanoneedles are further confirmed (Figure 1C, inset). High resolution (HR) TEM image (Figure 1D) shows a single nanoneedle with visible lattice fringes possessing an interplanar distance of about 0.33 nm, corresponding to the (110) plane of rutile TiO_2.[24,32]

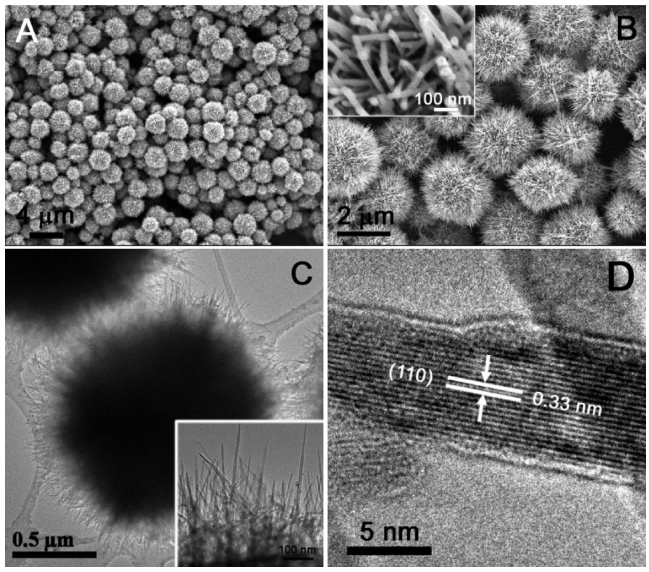

Figure 1. Scanning electron microscopy (SEM) images (A and B) of sample I synthesized at a low H_2O-to-EG ratio. Transmission electron microscopy (TEM) image (C) and high-resolution TEM image (D) of sample I. The insets in B and C show a magnified view of the nanoneedle subunits.

By increasing the H_2O-to-EG volume ratio, we are able to obtain urchinlike structure with a much smaller particle size (sample II). As shown in Figure 2A, sample II contains uniform and monodispersed particles with only a few hundred nanometers in size, which is much smaller than sample I. The particles also possess a unique structure consisting of urchinlike aggregation of thin nanoneedles with a diameter of about 400 nm (Figure 2B). The uniformity of the product is confirmed by TEM (Figure 2C). Moreover, the packing of the subunits are much looser than that of sample I (Figure 2D).

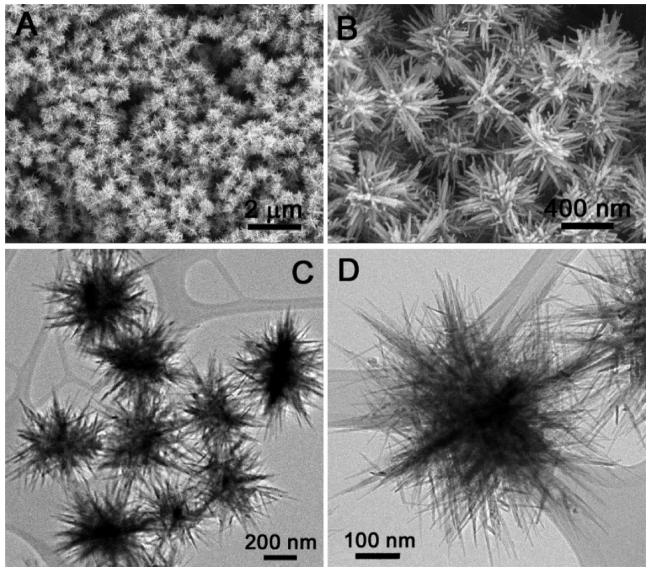

Figure 2. SEM (A and B) and TEM images (C and D) of sample II synthesized at a higher H_2O-to-EG ratio.

dx.doi.org/10.1021/am4022494 | ACS Appl. Mater. Interfaces 2013, 5, 9998−10003

The lattice spacings measured from HRTEM image (result not shown) suggests that the nanoneedle building blocks in sample II possess identical crystallographic structure compared to those of sample I.

The X-ray diffraction (XRD) patterns of the two samples are shown in Figure 3. All the identified peaks can be

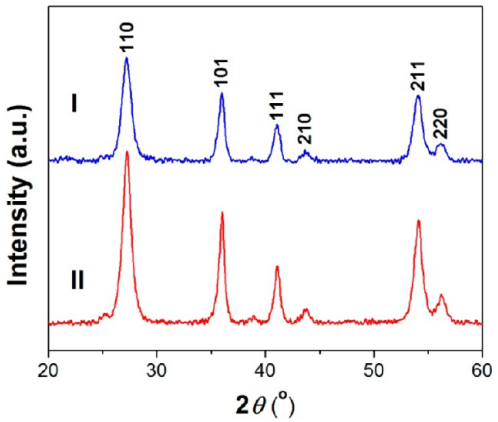

Figure 3. X-ray diffraction (XRD) patterns of sample I and II.

unambiguously assigned to the tetragonal rutile TiO_2 (JCPDS No. 21-1276, S.G.: $P4_2/mnm$, a_0 = 4.5933 Å, c_0 = 2.9592 Å).[32,40] The relatively high peak intensities suggest that both samples are of high crystallinity, which is consistent with the SEM and TEM results. Both samples have a similar surface area of about 80 $m^2\ g^{-1}$ (N_2 adsorption–desorption isotherms are shown in Figure 4). Sample I has a total pore volume and average pore size of 0.25 $cm^3\ g^{-1}$ and 14 nm, respectively; while those values for sample II are higher with 0.31 $cm^3\ g^{-1}$ and 16 nm, respectively. Both samples do not show a distinct hysteresis loop in their isotherms, suggesting that they do not possess a significant mesoporous structure. The thermogravimetric analysis (TGA) results (Figure 5) suggest that only negligible amount of organic compound is present in both samples, since there is a total weight loss of only about 6 wt % when the samples are heated up to 600 °C. Such a small weight change could be attributed to the decomposition of organic species absorbed on the sample, considering that there is large amount of EG in the synthesis system.

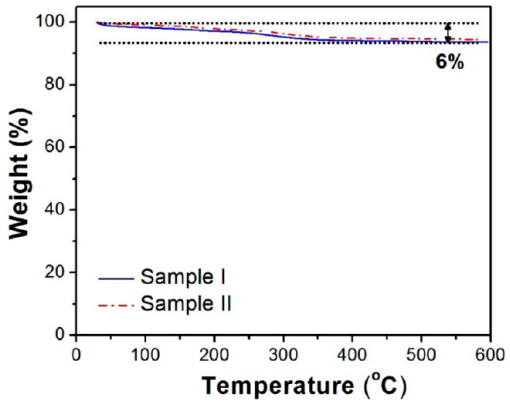

Figure 5. TGA results of the two samples. An insignificant weight loss of only 6% was observed in both samples.

Since concentration, time and temperature are all important parameters which would affect the morphology of our product, we performed a series of control experiments, in order to understand the formation mechanism of the urchinlike structure, and the results are shown in Supporting Information Figure S1. When the amount of either H_2O or EG was slightly changed, the sample appeared to have severely agglomerated and be less uniform, although the urchinlike structure could still be maintained (Supporting Information Figure S1A and B). In the cases when purely H_2O or EG was used in the synthesis, irregular particles were obtained (Supporting Information Figure S1C and D). Furthermore, replacing EG with diethylene glycol (DEG) resulted in the formation of aggregated rod-like particles (Supporting Information Figure S1E). If $TiCl_3$ was substituted by $TiCl_4$, nanorods with a much larger diameter were produced (Supporting Information Figure S1F). It is also important to mention that such an interesting urchinlike structure is very sensitive to experimental conditions, and any slight deviations from the current parameters will result in undesirable outcome. Based on the above observation, we propose a possible formation mechanism of our urchinlike structure. It has been documented that the transformation of $TiCl_3$ to TiO_2 consists of the following reactions:[24,32,41]

$$Ti^{3+} + H_2O \rightarrow TiOH^{2+} + H^+ \quad (1)$$

$$TiOH^{2+} + O_2 \rightarrow \text{Ti(IV) oxo species} + O_2 \rightarrow TiO_2 \quad (2)$$

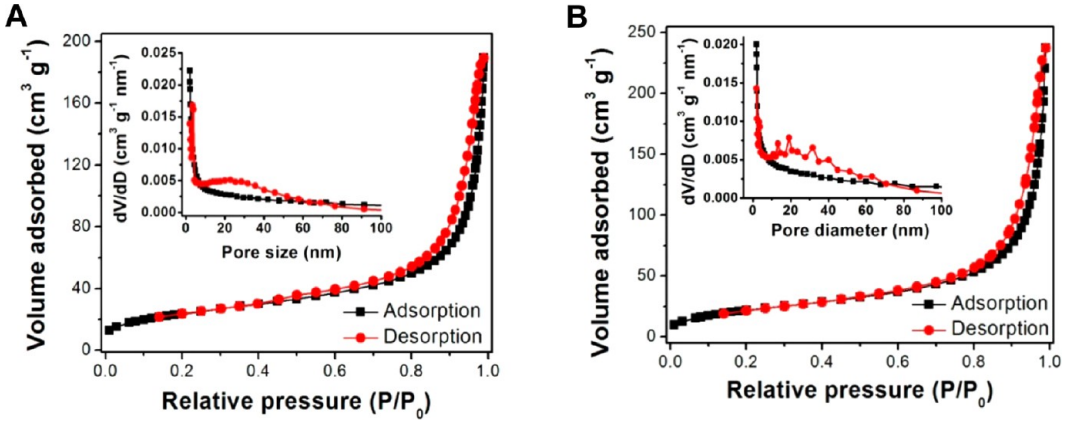

Figure 4. N_2 adsorption–desorption isotherms of sample I (A) and II (B). The insets show the Barrett–Joyner–Halenda pore size distribution from both branches of the isotherm. Both samples show similar surface areas of ~80 $m^2\ g^{-1}$.

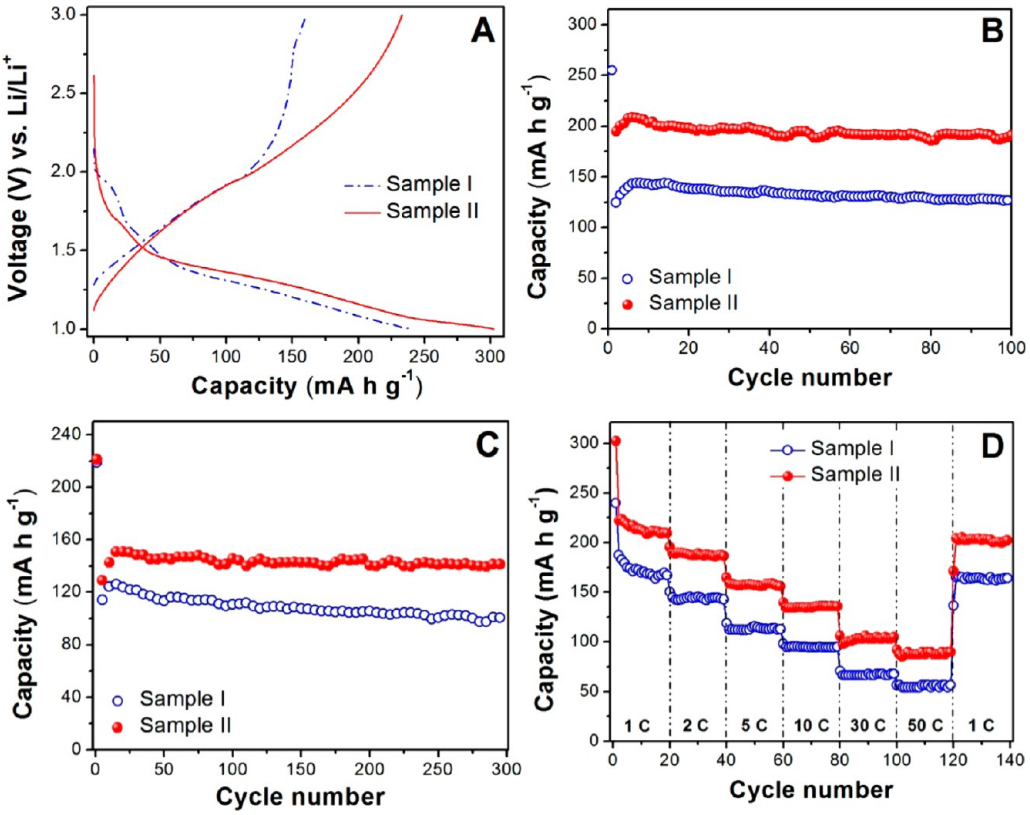

Figure 6. Comparative electrochemical measurements of sample I and II: Charge–discharge voltage profiles at a current rate of 1 C (A). Cycling performance at a constant current rate of 5 (B) and 10 C (C). Rate behavior at varying current rates from 1–50 C (D).

According to reaction 1, the hydrolysis of $TiCl_3$ only takes place in the H_2O phase of the current binary medium. As a result, the homogeneous mixture of EG and H_2O acts as an ideal environment for these Ti(IV) oxo species, rendering uniformly dispersed nucleation centers. It is thus conceivable that the volume ratio between EG and H_2O is crucial to the successful formation of the desired structure, and with a specific concentration of Ti^{3+}, any slight change in the concentration of either component creating minor disturbance to the balanced state of the mixture will lead to the aggregation of these nucleation centers, which eventually would result in nonuniform particles. Subsequently, the nuclei undergo a linear assembly and resulted in formation of 1D needle-like nanostructure. During the process, the large amount of EG serves as a structural directing agent and prohibits the lateral growth of the nuclei. The highly confined growth environment causes the as-formed ultrathin 1D subunits to self-organize into more stable 3D hierarchical structure, that is, urchinlike structure. This mechanism is consistent with our experimental result that sample I is relatively easier to grow into much larger particles than sample II, as the former possesses much higher nuclei concentration than that of later. It is worth mentioning that the O_2 in the Teflon container and the mixed solvent probably serves as the sole oxidant in the current system which helps the oxidation of Ti^{3+} to Ti^{4+}.

The lithium storage properties of the as-prepared samples were then evaluated. As shown in Figure 6A are the charge–discharge voltage profiles of the two samples at a current rate of 1 C. Sample I delivers a first-cycle discharge capacity of 240 mA h g^{-1}, with a corresponding charge capacity of 161 mA h g^{-1}. This leads to an irreversible capacity loss of 33%. Such a low Coulombic efficiency is commonly observed for nanosized rutile TiO_2,[16,20] which can be attributed to the trapping of inserted Li^+ after the large volume strain in the crystal structure.[19] On the other hand, much higher discharge and charge capacity of 302 and 233 mA h g^{-1} can be obtained for sample II, which leads to a significantly lower irreversible loss of only 22%. A small plateau region can be observed at about 1.7 V, which has been commonly identified in nanosized rutile TiO_2 based electrodes.[15,22] Figure 6B depicts the cyclic performance of the two samples at a constant current rate of 5 C. Both samples demonstrate good capacity retention up to 100 charge–discharge cycles, and sample II has a higher capacity of ~200 mA h g^{-1} compared to sample I with ~130 mA h g^{-1} at the end of the tests. Remarkably, at a much higher current rate of 10 C (Figure 6C), sample II exhibits excellent cyclic retention up to 300 cycles and a reversible capacity as high as ~140 mA h g^{-1} with a negligible loss of only 0.001% per cycle. Sample I also shows a very promising battery performance with a capacity of ~100 mA h g^{-1}. The rate behavior of the samples was further investigated by charging and discharging at varying current rates from 1 to 50 C (Figure 6D). Obviously, sample II possesses good cyclic stability at each current rate. Even at the highest current rate of 50 C (~8.5 A g^{-1}), a high capacity of 88 mA h g^{-1} can still be obtained. Furthermore, a stable capacity of ~200 mA h g^{-1}can still be delivered once the current rate is reduced back to 1 C, highlighting the good structural stability of the sample. For sample I, slightly lower capacities of 170, 145, 112, 95, 67, 55 mA h g^{-1} are delivered at 1, 2, 5, 10, 30, and 50 C, respectively. The performance of sample II is significantly better than other urchinlike rutile TiO_2 tested under the similar conditions,[23,24,39,42] and is also advantageous over rutile TiO_2 with other morphologies,[20,22,40] or even TiO_2 with different

dx.doi.org/10.1021/am4022494 | ACS Appl. Mater. Interfaces 2013, 5, 9998–10003

carbonaceous supports.[43−46] Considering both sample I and II have similar surface area and primary building blocks, such a magnificent performance of sample II could be attributed to its loose packing of the subunits. This important feature grants good carrier access into the central regions of the structure, leading to a better interaction with the electrolyte. Furthermore, the overall small particle size may also contribute to better electron and Li^+ transduction. On the other hand, sample I is shown to have a considerably larger particle size and a much denser packing of the rod-like subunits (compare Figure 1C and 2D). This might create a much weaker contact between the electrolyte and the central region of the particles, thus rendering the accessibility of electrons/Li^+ to these parts difficult. This could result in an incomplete interaction between the TiO_2 electrode and Li^+, which would probably lead to lower lithium storage capacities, as depicted in Figure 6. This hypothesis is actually confirmed by the BET analysis, as sample II has a higher total pore volume and average pore size than those of sample I. Further comparing to previously reported urchinlike rutile TiO_2 with a much lower surface area,[24] our samples exhibit significantly enhanced lithium storage properties, evidently showing the advantage of the unique urchinlike structure prepared by the current H_2O−EG system. It is thus conceivable that through tuning these material properties, including the morphology, particle size, organization of subunits, by proper nanostructuring, the performance of the material can be dramatically improved.

CONCLUSION

In summary, a green solvothermal method was developed in this work to synthesize uniform urchinlike rutile TiO_2 assembled from ultrathin nanoneedles. The mixed solvent of H_2O and EG provides an ideal environment for the formation of monodispersed particles with very uniform size distribution via regulating the nucleation and crystal growth of rutile TiO_2. The electrochemical results showed that the as-prepared samples possess superior lithium storage properties with a high reversible capacity of ∼140 mA h g^{-1} at a high current rate of 10 C upon prolonged cycling up to 300 cycles. The almost unmatched battery performance highlighted that rutile TiO_2 may have as great potential as its anatase counterpart in electrochemical applications which can be realized by intelligent nanostructuring.

ASSOCIATED CONTENT

Supporting Information

FESEM images showing the morphology of samples prepared in control experiments. This information is available free of charge via the Internet at http://pubs.acs.org/.

AUTHOR INFORMATION

Corresponding Author

*E-mail: asxhu@ntu.edu.sg.

Notes

The authors declare no competing financial interest.

ACKNOWLEDGMENTS

The authors wish to thank National Research Foundation (NRF) and A-Star Singapore for supporting the research projects on structural and functional nanomaterials.

REFERENCES

(1) Armand, M.; Tarascon, J. M. *Nature* **2008**, *451*, 652−657.
(2) Tarascon, J. M.; Armand, M. *Nature* **2001**, *414*, 359−367.
(3) Bruce, P. G.; Scrosati, B.; Tarascon, J. M. *Angew. Chem., Int. Ed.* **2008**, *47*, 2930−2946.
(4) Goodenough, J. B.; Kim, Y. *Chem. Mater.* **2009**, *22*, 587−603.
(5) Larcher, D.; Beattie, S.; Morcrette, M.; Edstrom, K.; Jumas, J.-C.; Tarascon, J.-M. *J. Mater. Chem.* **2007**, *17*, 3759−3772.
(6) Cheng, F.; Tao, Z.; Liang, J.; Chen, J. *Chem. Mater.* **2007**, *20*, 667−681.
(7) Zheng, X. T.; Li, C. M. *Chem. Soc. Rev.* **2011**, *41*, 2061−2071.
(8) Wen, C. Z.; Jiang, H. B.; Qiao, S. Z.; Yang, H. G.; Lu, G. Q. *J. Mater. Chem.* **2011**, *21*, 7052−7061.
(9) Chen, J. S.; Liu, J.; Qiao, S. Z.; Xu, R.; Lou, X. W. *Chem. Commun.* **2011**, *47*, 10443−10445.
(10) Deng, D.; Kim, M. G.; Lee, J. Y.; Cho, J. *Energy Environ. Sci.* **2009**, *2*, 818−837.
(11) Ding, S. J.; Chen, J. S.; Luan, D. Y.; Boey, F. Y. C.; Madhavi, S.; Lou, X. W. *Chem. Commun.* **2011**, *47*, 5780−5782.
(12) Wu, H. B.; Chen, J. S.; Hng, H. H.; Lou, X. W. *Nanoscale* **2012**, *4*, 2526−2542.
(13) Chen, J. S.; Lou, X. W. *Mater. Today* **2012**, *15*, 246−254.
(14) Yang, Z. G.; Choi, D.; Kerisit, S.; Rosso, K. M.; Wang, D. H.; Zhang, J.; Graff, G.; Liu, J. *J. Power Sources* **2009**, *192*, 588−598.
(15) Chen, J. S.; Lou, X. W. *J. Power Sources* **2010**, *195*, 2905−2908.
(16) Baudrin, E.; Cassaignon, S.; Koesch, M.; Jolivet, J. P.; Dupont, L.; Tarascon, J. M. *Electrochem. Commun.* **2007**, *9*, 337−342.
(17) Borghols, W. J. H.; Wagemaker, M.; Lafont, U.; Kelder, E. M.; Mulder, F. M. *Chem. Mater.* **2008**, *20*, 2949−2955.
(18) Macklin, W. J.; Neat, R. J. *Solid State Ionics* **2003**, *53*−*56*, 694−700.
(19) Vijayakumar, M.; Kerisit, S.; Wang, C. M.; Nie, Z. M.; Rosso, K. M.; Yang, Z. G.; Graff, G.; Liu, J.; Hu, J. Z. *J. Phys. Chem. C* **2009**, *113*, 14567−14574.
(20) Hu, Y. S.; Kienle, L.; Guo, Y. G.; Maier, J. *Adv. Mater.* **2006**, *18*, 1421−1426.
(21) Jiang, C. H.; Honma, I.; Kudo, T.; Zhou, H. S. *Electrochem. Solid State Lett.* **2007**, *10*, A127−A129.
(22) Wang, D.; Choi, D.; Yang, Z.; Viswanathan, V. V.; Nie, Z.; Wang, C.; Song, Y.; Zhang, J.-G.; Liu, J. *Chem. Mater.* **2008**, *20*, 3435−3442.
(23) Li, J. M.; Wan, W.; Zhu, F.; Li, Q.; Zhou, H. H.; Li, J. J.; Xu, D. S. *Chem. Commun.* **2012**, *48*, 389−391.
(24) Park, K.-S.; Min, K.-M.; Jin, Y.-H.; Seo, S.-D.; Lee, G.-H.; Shim, H.-W.; Kim, D.-W. *J. Mater. Chem.* **2012**, *22*, 15981−15986.
(25) Kong, E.-H.; Chang, Y.-J.; Park, Y.-C.; Yoon, Y.-H.; Park, H.-J.; Jang, H. M. *Phys. Chem. Chem. Phys.* **2012**, *14*, 4620−4625.
(26) Xiang, L. Q.; Zhao, X. P.; Yin, J. B.; Fan, B. L. *J. Mater. Sci.* **2012**, *47*, 1436−1445.
(27) Hayashi, K.; Nakamura, M.; Makita, Y.; Fujiwara, R.; Kori, T.; Ishimura, K. *Mater. Lett.* **2011**, *65*, 3037−3040.
(28) Wu, J. M.; Song, X. M.; Yan, M. *J. Hazard. Mater.* **2011**, *194*, 338−344.
(29) Cheng, Q. L.; Pavlinek, V.; He, Y.; Yan, Y. F.; Li, C. Z.; Saha, P. *Colloid Polym. Sci.* **2011**, *289*, 799−805.
(30) Bai, X. L.; Xie, B.; Pan, N.; Wang, X. P.; Wang, H. Q. *J. Solid State Chem.* **2008**, *181*, 450−456.
(31) Liu, B.; Zeng, H. C. *J. Am. Chem. Soc.* **2004**, *126*, 16744−16746.
(32) Hosono, E.; Fujihara, S.; Kakiuchi, K.; Imai, H. *J. Am. Chem. Soc.* **2004**, *126*, 7790−7791.
(33) Bae, E.; Ohno, T. *Appl. Catal., B* **2009**, *91*, 634−639.
(34) Kakiuchi, K.; Hosono, E.; Imai, H.; Kimura, T.; Fujihara, S. *J. Cryst. Growth* **2006**, *293*, 541−545.
(35) Li, X.; Xiong, Y.; Li, Z.; Xie, Y. *Inorg. Chem.* **2006**, *45*, 3493−3495.
(36) Santulli, A. C.; Koenigsmann, C.; Tiano, A. L.; DeRosa, D.; Wong, S. S. *Nanotechnology* **2011**, *22*, 245402.
(37) Zhu, F.; Wu, D.; Li, Q.; Dong, H.; Li, J.; Jiang, K.; Xu, D. *RSC Adv.* **2012**, *2*, 11629−11637.

(38) Sun, Z.; Kim, J. H.; Zhao, Y.; Bijarbooneh, F.; Malgras, V.; Lee, Y.; Kang, Y.-M.; Dou, S. X. *J. Am. Chem. Soc.* **2011**, *133*, 19314−19317.
(39) Yoon, S.; Manthiram, A. *J. Phys. Chem. C* **2011**, *115*, 9410−9416.
(40) Chen, J. S.; Lou, X. W. *Chem. Sci.* **2011**, *2*, 2219−2223.
(41) Rotzinger, F. P.; Graetzel, M. *Inorg. Chem.* **1987**, *26*, 3704−3708.
(42) Qiao, H.; Wang, Y. W.; Xiao, L. F.; Zhang, L. Z. *Electrochem. Commun.* **2008**, *10*, 1280−1283.
(43) Das, S. K.; Darmakolla, S.; Bhattacharyya, A. J. *J. Mater. Chem.* **2010**, *20*, 1600−1606.
(44) Moriguchi, I.; Hidaka, R.; Yamada, H.; Kudo, T.; Murakami, H.; Nakashima, N. *Adv. Mater.* **2006**, *18*, 69−73.
(45) Das, S. K.; Bhattacharyya, A. J. *J. Phys. Chem. C* **2009**, *113*, 17367−17371.
(46) Chen, J. S.; Liu, H.; Qiao, S. Z.; Lou, X. W. *J. Mater. Chem.* **2011**, *21*, 5687−5692.